Substrate considerations for CIGS (key issues)

- Earlier CIS or CIGS devices were fabricated on borosilicate glass. Switching to less-expensive soda lime glass, the solar cells worked better (i.e., higher efficiency).
- *Why does soda lime glass work well for CIS / CIGS*?
- **Coefficient of thermal expansion**: deposition done at a substrate temperature T_{SS} > 350 °C and as high as T_{SS} ~ 550 °C (close to the glass transition temp of ~564 °C). Subsequent cooling of the substrate introduces significant strain if coefficient of thermal expansion differ for the thin film and the substrate. Fortuitously, soda lime glass has a value for the thermal expansion coefficient of 9.5 (ppm/K); the value for CIS is ~8 ppm/K. In contrast, borosilicate glass has a value of 4.6 ppm/K.
- Soda lime glass includes oxides such as Na_2O, K_2O, and CaO, which provide **sources of alkali impurities** which diffuse into the Mo and Cu(InGa)Se_2 films resulting in beneficial defect effects.
- Alkalai impurities are better introduced through a controlled source, so now the glass is coated with a Na diffusion barrier such as SiO_x or Al_2O_3.
- "The chalcopyrite phase field is increased by the addition of Ga or Na." This means that the desirable phase of CIS (or CIGS) is more easily achieved in the presence of Na.

Cu(InGa)Se_2 Solar Cells, by William N. Shafarman[1] and Lars Stolt[2]
[1]*University of Delaware, Newark, DE, USA,* [2]*Uppsala University, Uppsala, Sweden*
Handbook of Photovoltaic Science and Engineering. Edited by A. Luque and S. Hegedus
2003 John Wiley & Sons, Ltd ISBN: 0-471-49196-9

Soda lime glass transmission

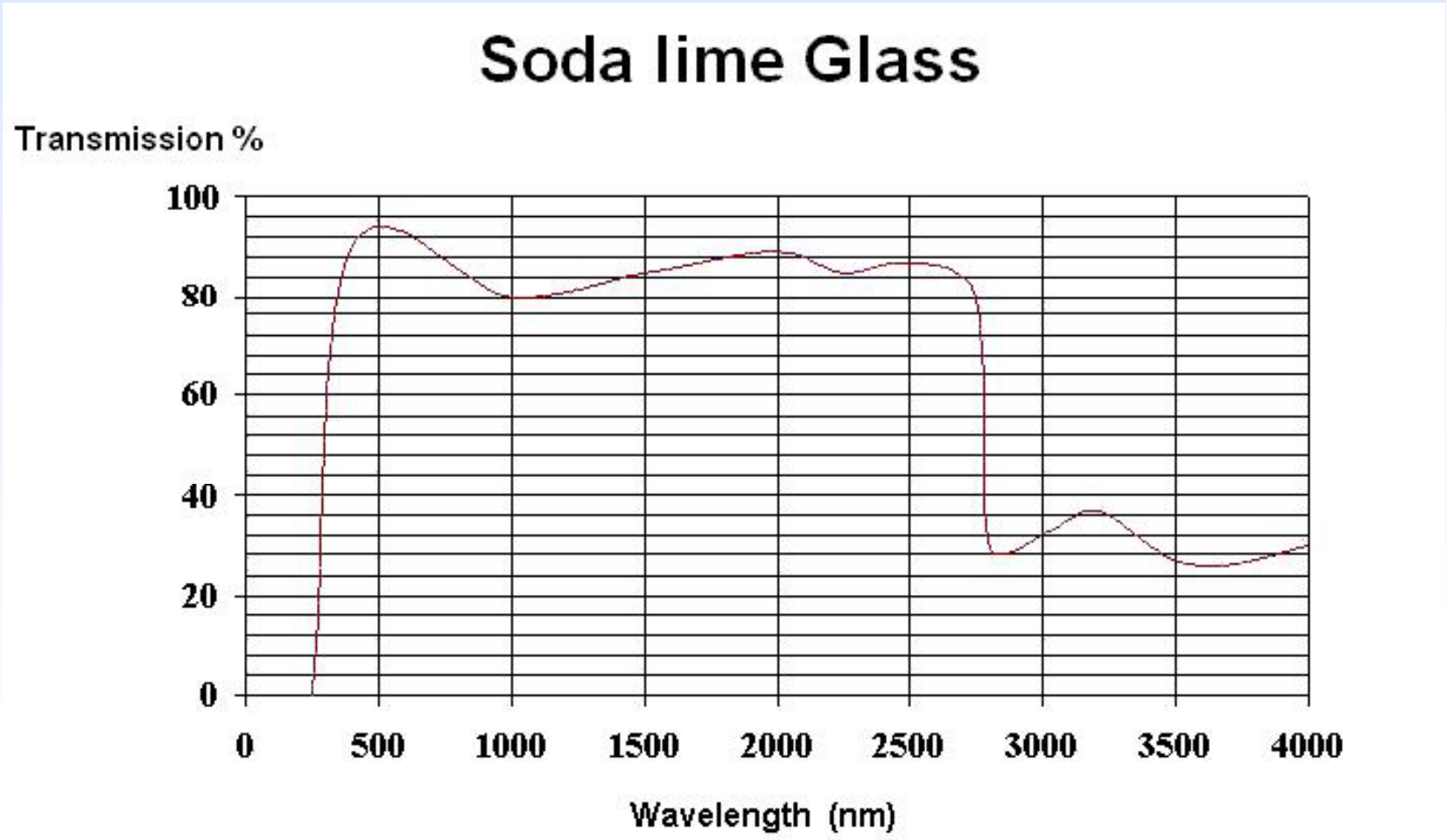

http://en.wikipedia.org/wiki/File:Soda_Lime.jpg

Soda lime glass properties

Properties	Soda-lime glass for windows
Chemical composition, (wt%)	73 SiO_2, 14 Na_2O, 9 CaO, 4 MgO, 0.15 Al_2O_3, 0.03 K_2O, 0.02 TiO_2, 0.1 Fe_2O_3
Glass transition temperature, T_g, °C	564
Coefficient of thermal expansion, ppm/K, ~100-300°C	9.5
Refractive index, n_D at 20°C	1.520
Heat capacity at 20°C, J/(mol·K)	*48*

http://en.wikipedia.org/wiki/Soda-lime_glass

CIGS back contact (molybdenum, Mo)

- All high-efficiency CIS and CIGS devices use Mo as the back contact.
- Typically deposited by DC sputtering.
- Cell or module configuration determines required thickness (1 µm gives a sheet resistance of 0.1 to 0.2 Ω /□, *a factor of 2 to 4 higher resistivity* than bulk Mo.
- Sputter deposition requires careful control of the pressure to control stress in the film, to avoid adhesion problems.
- During Cu(InGa)Se_2 deposition, a $MoSe_2$ layer forms at the interface, with properties influenced by the Mo film (less $MoSe_2$ forms on dense Mo). Metals other than Mo have been investigated with limited success.

Cu(InGa)Se_2 Solar Cells, by William N. Shafarman[1] and Lars Stolt[2]
[1]*University of Delaware, Newark, DE, USA,* [2]*Uppsala University, Uppsala, Sweden*
Handbook of Photovoltaic Science and Engineering. Edited by A. Luque and S. Hegedus
2003 John Wiley & Sons, Ltd ISBN: 0-471-49196-9

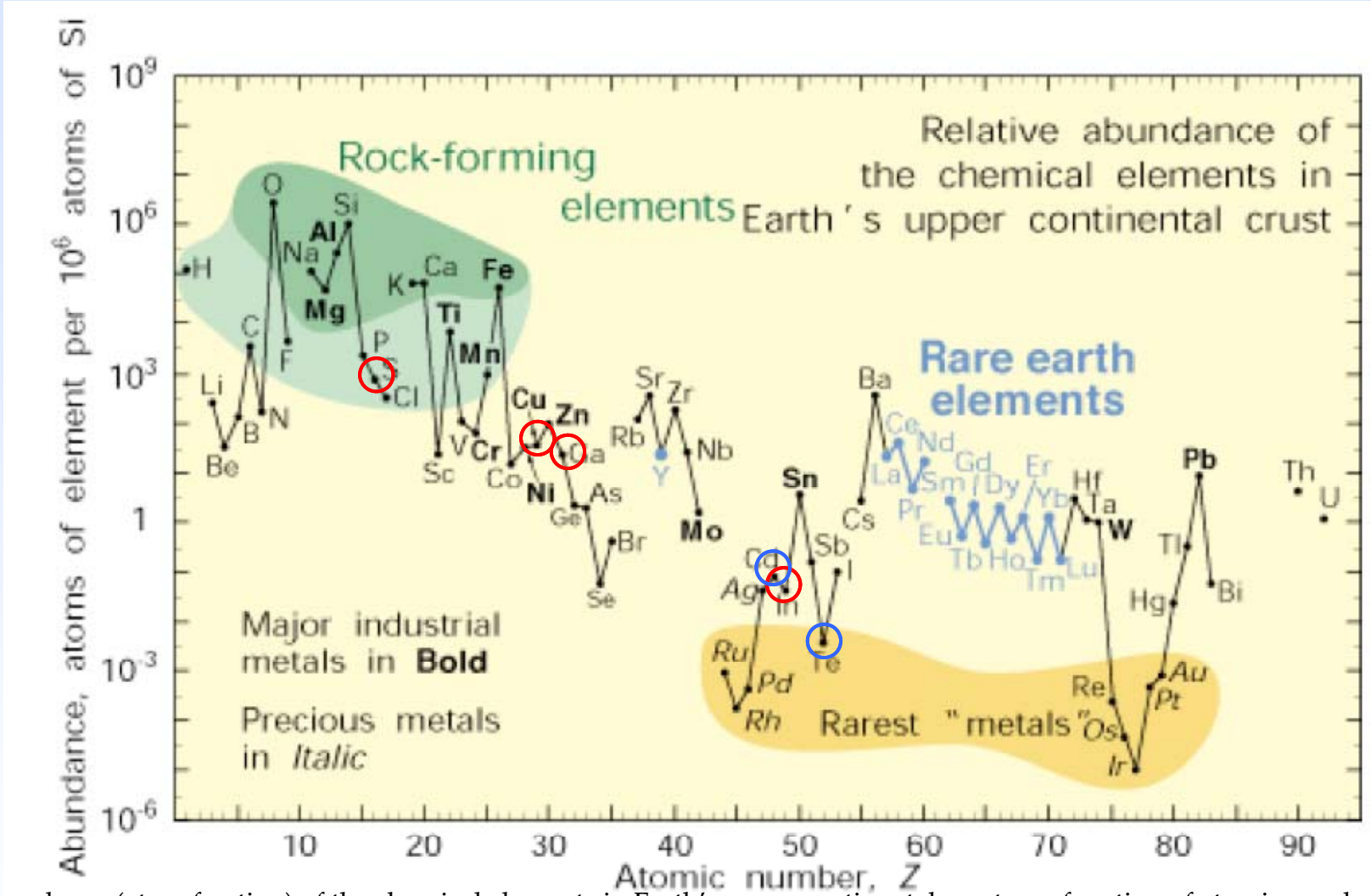

Abundance (atom fraction) of the chemical elements in Earth's upper continental crust as a function of atomic number. Many of the elements are classified into (partially overlapping) categories: (1) rock-forming elements (major elements in green field and minor elements in light green field); (2) rare earth elements (lanthanides, La–Lu, and Y; labeled in blue); (3) major industrial metals (global production >~3×10^7 kg/year; labeled in bold); (4) precious metals (italic); and (5) the nine rarest "metals"—the six platinum group elements plus Au, Re, and Te (a metalloid)

Gordon B. Haxel, James B. Hedrick, and Greta J. Orris, Rare Earth Elements—Critical Resources for High Technology, U.S. Geological Survey Fact Sheet 087-02

http://pubs.usgs.gov/fs/2002/fs087-02/

State of Commercialization, as of 2003

Several companies worldwide are pursuing the commercial development of Cu(InGa)Se2-based modules. The most advanced, having demonstrated excellent reproducibility in its module manufacturing using the two-stage selenization process for Cu(InGa)(SeS)2 deposition is Shell Solar Industries (SSI) in California, which was formerly ARCO Solar and then Siemens Solar. They are now in production with 5-, 10-, 20-, and 40-W modules that are commercially available.

In Germany, Wurth Solar is in pilot production using an in-line coevaporation process for Cu(InGa)Se2 deposition and has also reported large area modules with >12% efficiency. In the USA, several companies are in preproduction or pilot production: Energy Photovoltaics, Inc. (EPV) is using its own in-line evaporation process, International Solar Electric Technology (ISET) is developing a particle-based precursor for selenization, and Global Solar Energy (GSE) is pursuing a process for roll-to-roll coevaporation onto a flexible substrate. In Japan, Showa Shell, using a two-stage selenization process, and Matsushita, using coevaporation for Cu(InGa)Se2 deposition, are also in production development stages.

Despite the level of effort on developing manufacturing processes, there remains a large discrepancy in efficiency between the laboratory-scale solar cells and minimodules, and the best full-scale modules. In part, this is due to the necessity for developing completely new processes and equipment for the large-area, high-throughput deposition needed for manufacturing thin-film photovoltaics. This is compounded by the lack of a comprehensive scientific base for Cu(InGa)Se2 materials and devices, due partly to the fact that it has not attracted a broader interest for other applications. This lack of a science base has been perhaps the biggest hindrance to the maturation of Cu(InGa)Se2 solar cell technology as most of the progress has been empirical. Still, in many areas a deeper understanding has emerged in the recent years.

After "Cu(InGa)Se_2 Solar Cells", by Shafarman and Stolt, and *Wikipedia*

Solar Cell Materials and Device Characterization (continued)

March 31, 2011

The University of Toledo, Department of Physics and Astronomy
SSARE, PVIC

Principles and Varieties of Solar Energy (PHYS 4400)
and
Fundamentals of Solar Cells (PHYS 6980)

Requirements/conditions for constructing a valuable solar cell

A partial list…

- Absorb sunlight efficiently to optimize photogeneration of carriers
- Achieve charge separation, directing electron and holes to different contacts (e.g., use doped materials for p-n junction)
- Demonstrate strongly rectifying (diode) behavior
- Avoid excessive electron-hole recombination within the solar cell (maximize photocurrent)
- Maintain as much of the electric potential as possible (avoid resistive losses, and optimize energy band offsets)
- Resist/avoid degradation by air and water (sealing the modules is often essential) – i.e. achieve stability
- Do all of these things (a) with high yield, (b) inexpensively, and c) at very large production levels
- What else?

More on characterization…

- Raman spectroscopy
- TGA/DSC
- XRD
- UPS
- FTIR
- Carrier lifetime measurements (TRPL, TA, TRMC, Ultrahigh Frequency Photoconductive Decay)
- TEM (Transmission Electron Microscopy)
- SEM (Scanning Electron Microscopy)
- EDS (Energy Dispersive Spectroscopy)
- AES (Auger Electron Spectroscopy)
- Resonance-Coupled Photoconductive Decay (RCPCD)
-

This list will eventually contain <u>many</u> more entries. The art of efficiently pursuing scientific understanding and technical knowledge resides in familiarity with the characterization "toolchest" and knowing which techniques to choose for specific problems/goals. Often a complement of methods is necessary to fully clarify mechanisms and properties.

Ultraviolet Photoelectron Spectroscopy

UPS is a type of Photoemission Spectroscopy…

Work function of indium tin oxide transparent conductor measured by photoelectron spectroscopy

Y. Park,[a] V. Choong, and Y. Gao
Department of Physics and Astronomy, University of Rochester, Rochester, New York 14627

B. R. Hsieh
Xerox Co., Wilson Center for Research and Technology, 14-39D, Webster, New York 14580

C. W. Tang
Imaging Research and Advanced Development, Eastman Kodak Co., Rochester, New York 14650

(Received 11 January 1996; accepted for publication 4 March 1996)

We used ultraviolet and x-ray photoelectron spectroscopy (XPS) and (UPS) techniques to directly measure absolute values of vacuum work function of indium tin oxide (ITO) thin films. We obtained a work function of 4.4–4.5 eV which is lower than the commonly cited value. These values do not change substantially by heating and Ar ion sputtering. The atomic concentrations of each element in ITO, measured with XPS, are also quite stable under heat treatment and ion sputtering. © *1996 American Institute of Physics.* [S0003-6951(96)04219-2]

Appl. Phys. Lett. **68 (19), 6 May 1996**

Ultraviolet Photoelectron Spectroscopy

High vacuum required for both UV (He I line at 58.4 nm) and detection of photoelectron

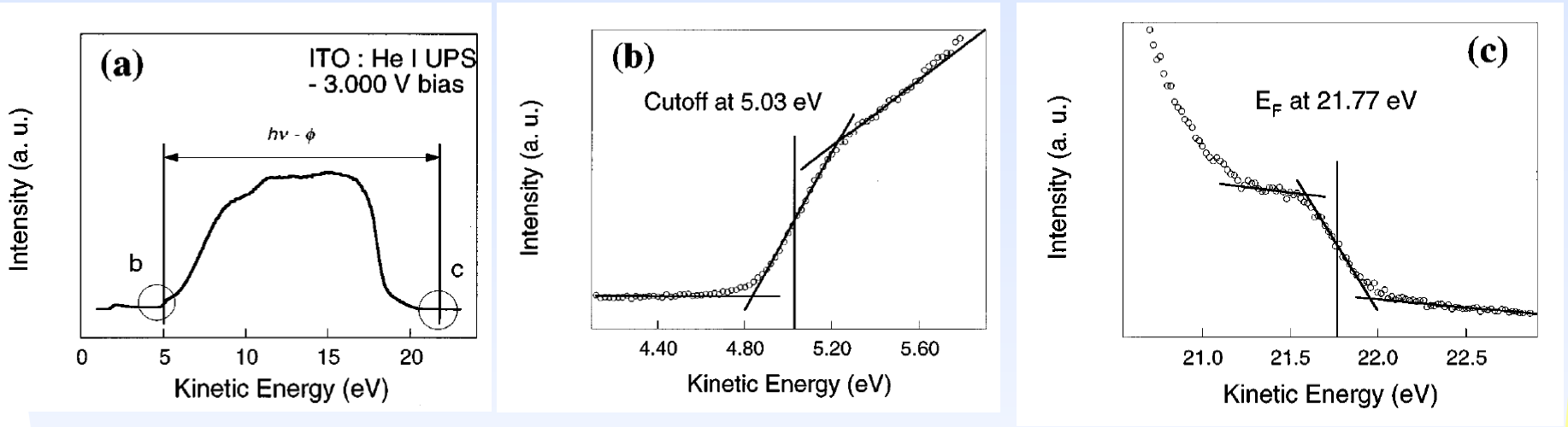

"(a) Shows a typical He I ($h\nu$ = 21.22 eV) UPS spectrum of ITO taken with -3.00 V bias applied to the sample. Also shown is inelastic cutoff (b) and Fermi edge (c). The relation between spectrum width $h\nu$, and work function φ is illustrated. (b) Shows a detailed spectrum of inelastic cutoff region. It also shows the cutoff energy with a vertical bar; (c) is similar to (b), but shows Fermi edge region."

$(h\nu) - ((\text{Fermi edge cut-off}) - (\text{inelastic cut-off})) = 21.22 - (21.77 - 5.03) = 4.48 \text{ eV} = \varphi$

Spectrometer resolution and thermal effects broaden the spectrum and blur the cut-offs

Appl. Phys. Lett. **68 (19), 6 May 1996**

X-Ray Generation

X-rays are electromagnetic radiation with wavelength ~1 Å = 10^{-10} m (visible light ~5.5x10^{-7} m)

X-ray generation

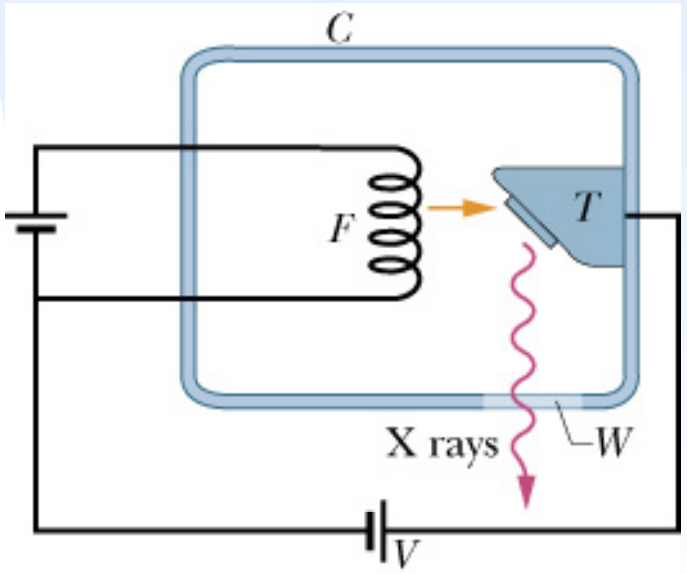

X-ray wavelengths too short to be resolved by a standard optical grating

$$\theta = \sin^{-1}\frac{m\lambda}{d} = \sin^{-1}\frac{(1)(0.1\text{ nm})}{3000\text{ nm}} = 0.0019°$$

X-Ray Generation

The most common metal used is copper, which can be kept cool easily, due to its high thermal conductivity, and which produces strong K_α and K_β lines. The K_β line is sometimes suppressed with a thin (~10 µm) nickel foil.

- **K-alpha (K_α)** emission lines result when an electron transitions to the innermost "K" shell (principal quantum number 1) from a 2p orbital of the second or "L" shell (with principal quantum number 2).

- The K_α line is actually a doublet, with slightly different energies depending on spin-orbit interaction energy between the electron spin and the orbital momentum of the 2p orbital.

$\lambda(K_\alpha)$ = 0.154 nm

$\lambda(K_\beta)$ = 0.139 nm

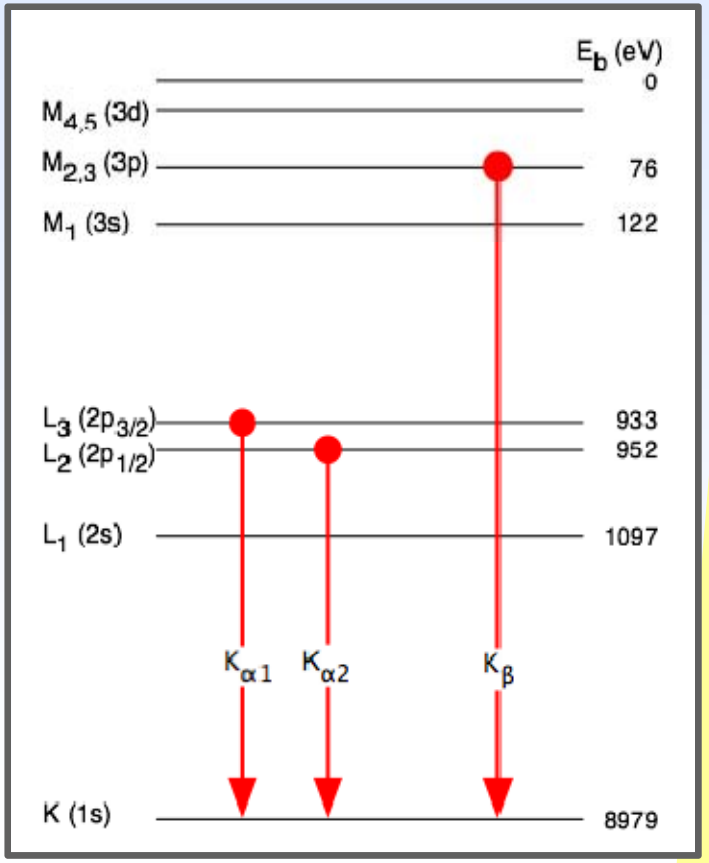

Atomic levels involved in copper K_α and K_β emission.

from http://en.wikipedia.org/wiki/K-alpha

K_α and K_β X-ray lines

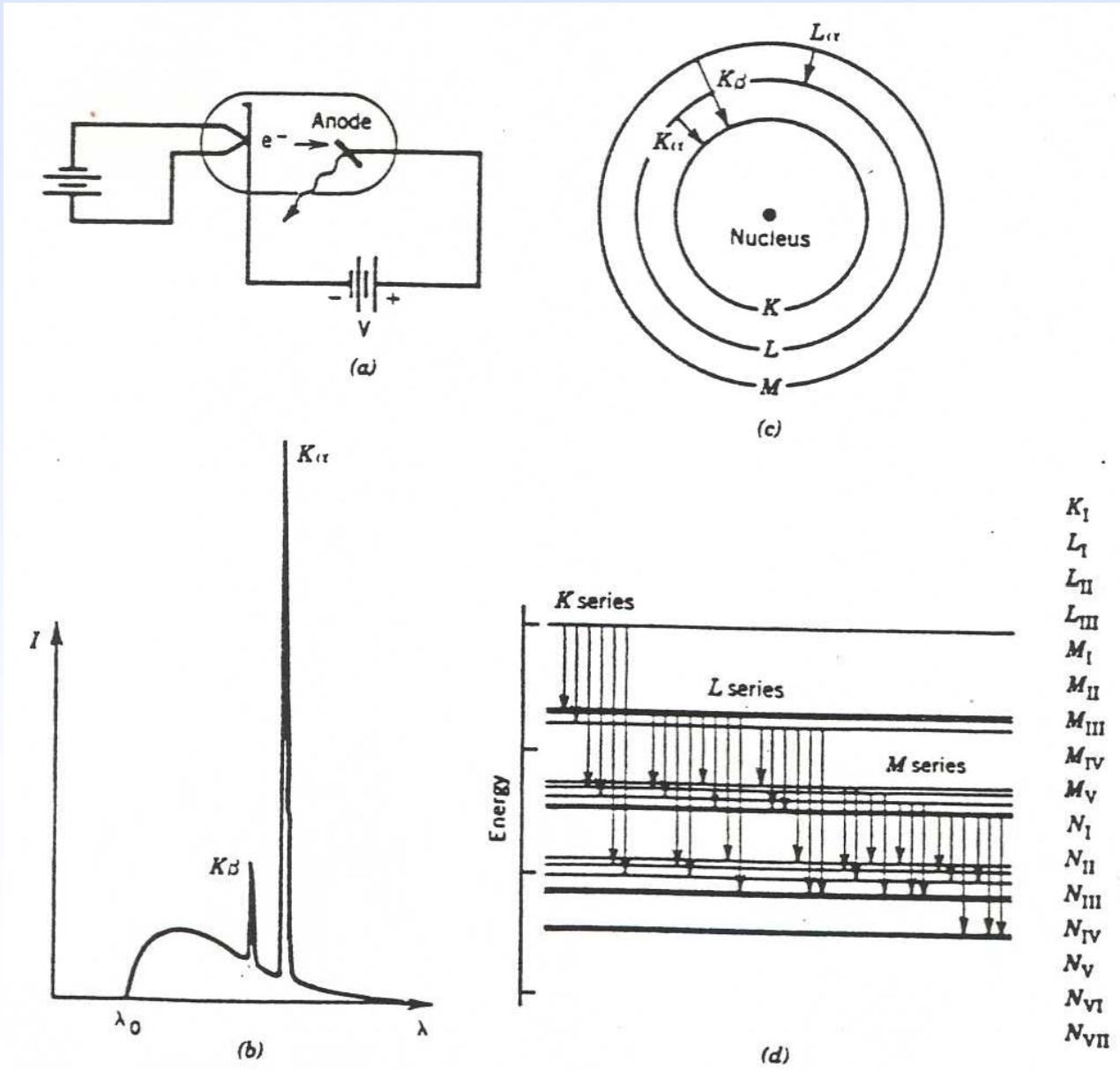

from Preston and Dietz, p. 191.

X-Ray diffraction – constructive interference

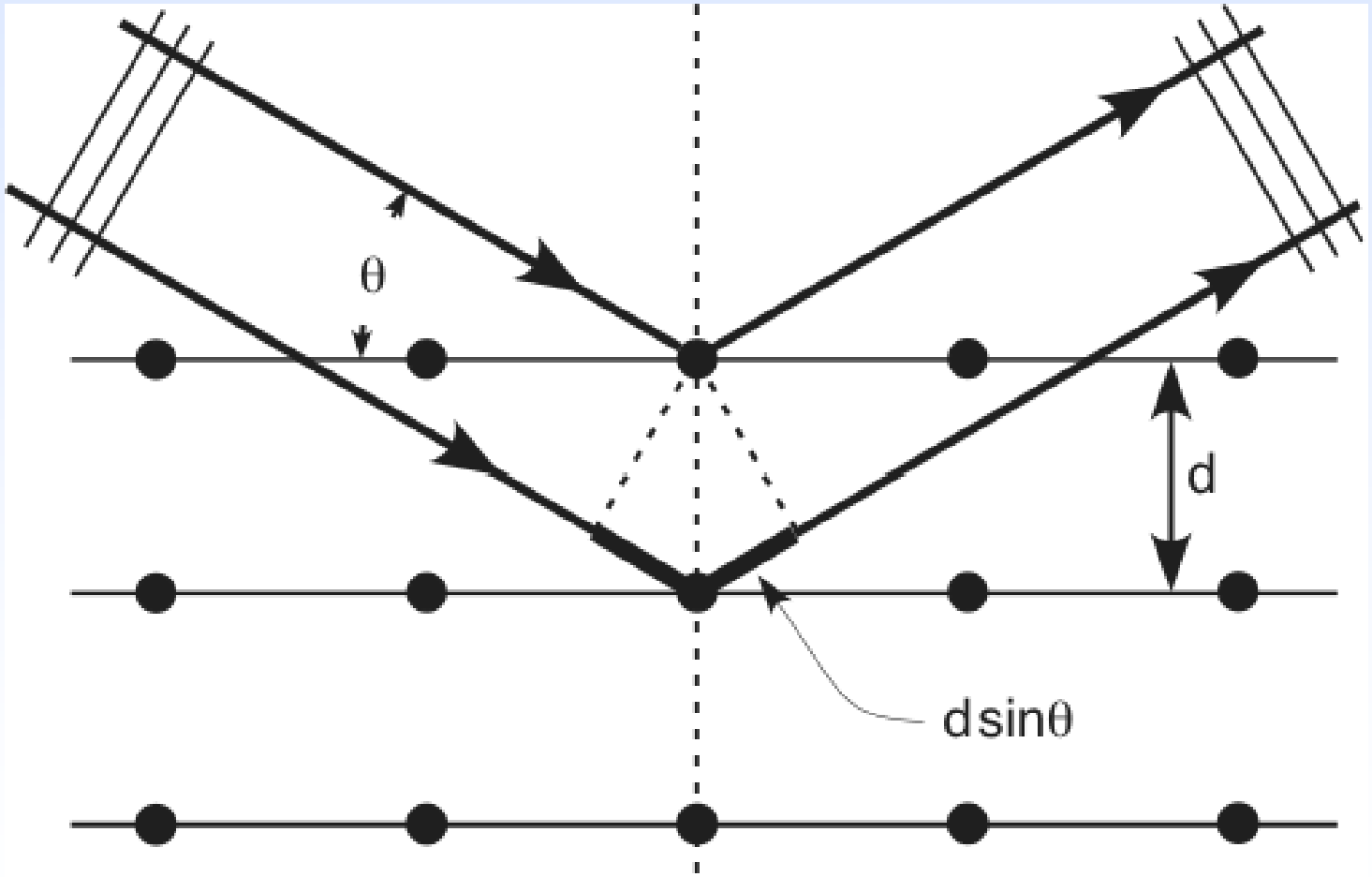

X-Ray Diffraction -- Bragg's Law

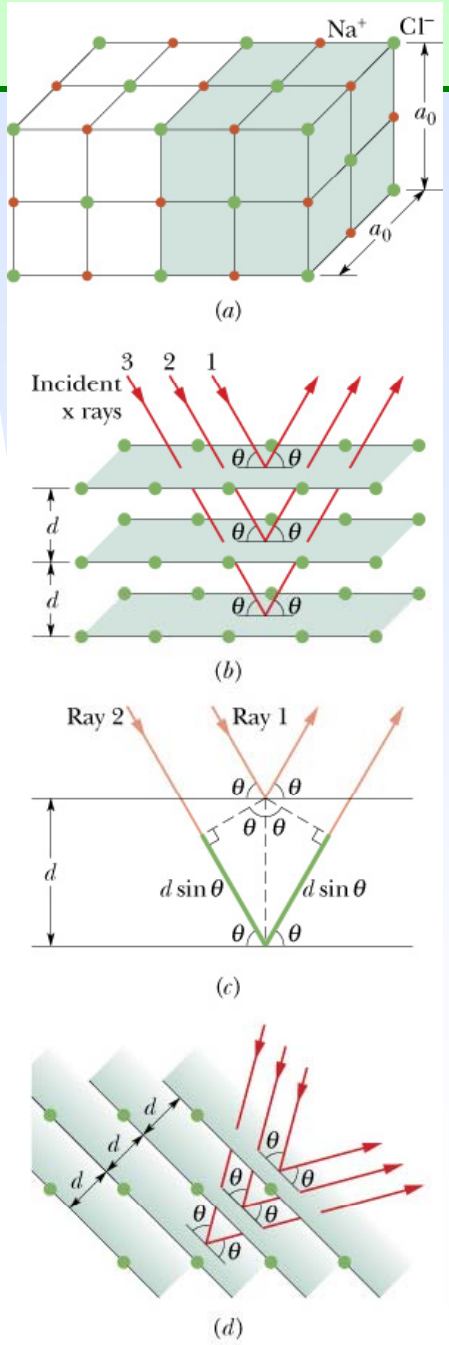

Diffraction of x-rays by crystal: spacing d of adjacent crystal planes on the order of 0.1 nm

→ three-dimensional diffraction grating with diffraction maxima along angles where reflections from different planes interfere constructively

$$2d \sin\theta = m\lambda \text{ for } m = 0, 1, 2, \ldots$$

Bragg's Law

The Braggs (Bragg's Law)

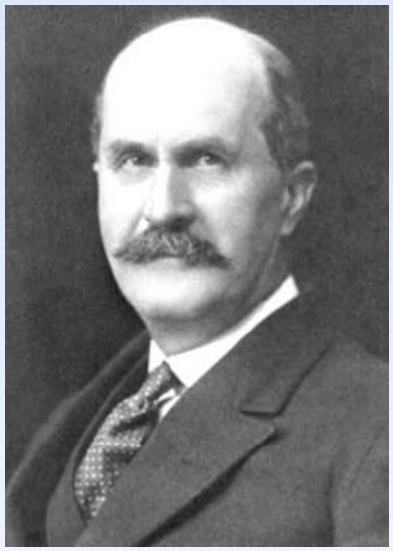

Sir William Henry Bragg
1862 - 1942

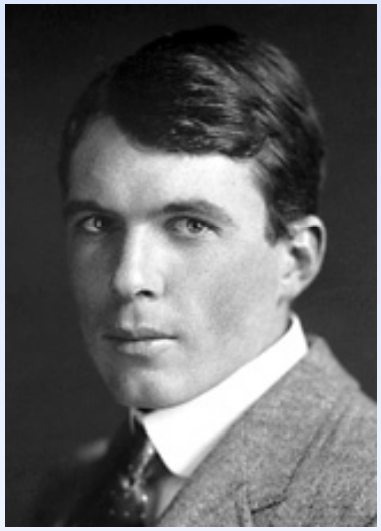

William Lawrence Bragg
1890 - 1971

Bragg occupied the Cavendish chair of physics at the University of Leeds from 1909. He continued his work on X-rays with much success. He invented the X-ray spectrometer and with his son, William Lawrence Bragg, then a research student at Cambridge, founded the new science of X-ray analysis of crystal structure.

In 1915 father and son were jointly awarded the Nobel Prize in Physics for their studies, using the X-ray spectrometer, of X-ray spectra, X-ray diffraction, and of crystal structure.

http://en.wikipedia.org/wiki/William_Henry_Bragg

X-Ray Diffraction, cont'd

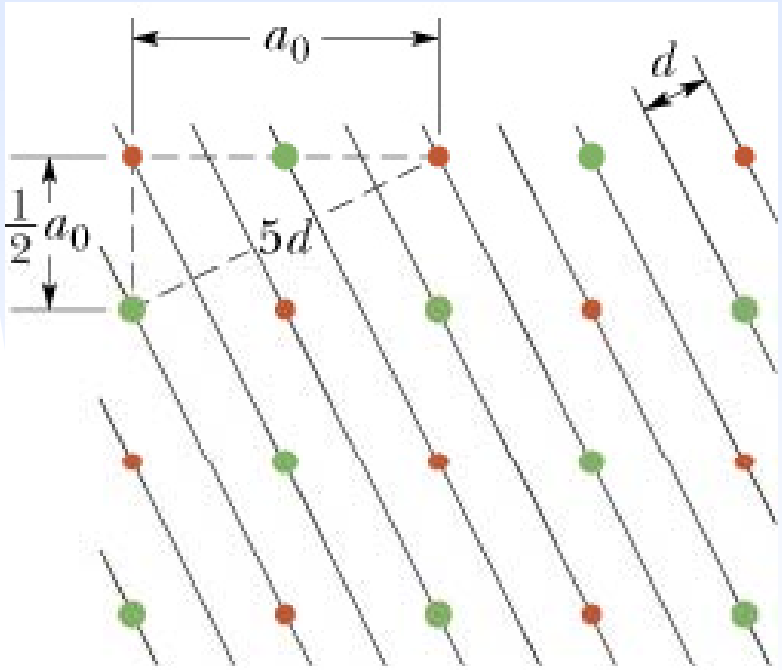

Interplanar spacing d is related to the unit cell dimension a_0

$$5d = \sqrt{\tfrac{5}{4}a_0^2} \quad \text{or} \quad d = \frac{a_0}{20} = 0.2236a_0$$

Not only can crystals be used to separate different x-ray wavelengths, but x-rays in turn can be used to study crystals, for example determine the type of crystal ordering and a_0.

Rock salt (cubic) crystal structure

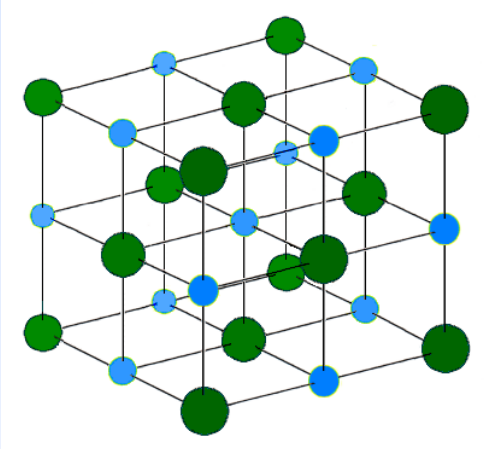

$$d_{hkl} = \frac{a_0}{\sqrt{h^2 + k^2 + l^2}}$$

Structure factor for NaCl:

$$F = \left[f_{Na} + f_{Cl} e^{i\pi(h+k+l)} \right] \left[1 + e^{i\pi(h+k)} + e^{i\pi(h+l)} + e^{i\pi(k+l)} \right]$$

$$\begin{aligned} F &= 4\left(f_{Na} + f_{Cl} \right) && \text{if } h, k, l \text{ are even} \\ F &= 4\left(f_{Na} - f_{Cl} \right) && \text{if } h, k, l \text{ are odd} \\ F &= 0 && \text{if } h, k, l \text{ are mixed} \end{aligned}$$

X-Ray diffraction (XRD) pattern (diffractogram) from NaCl

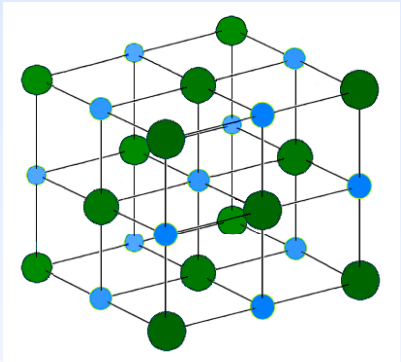

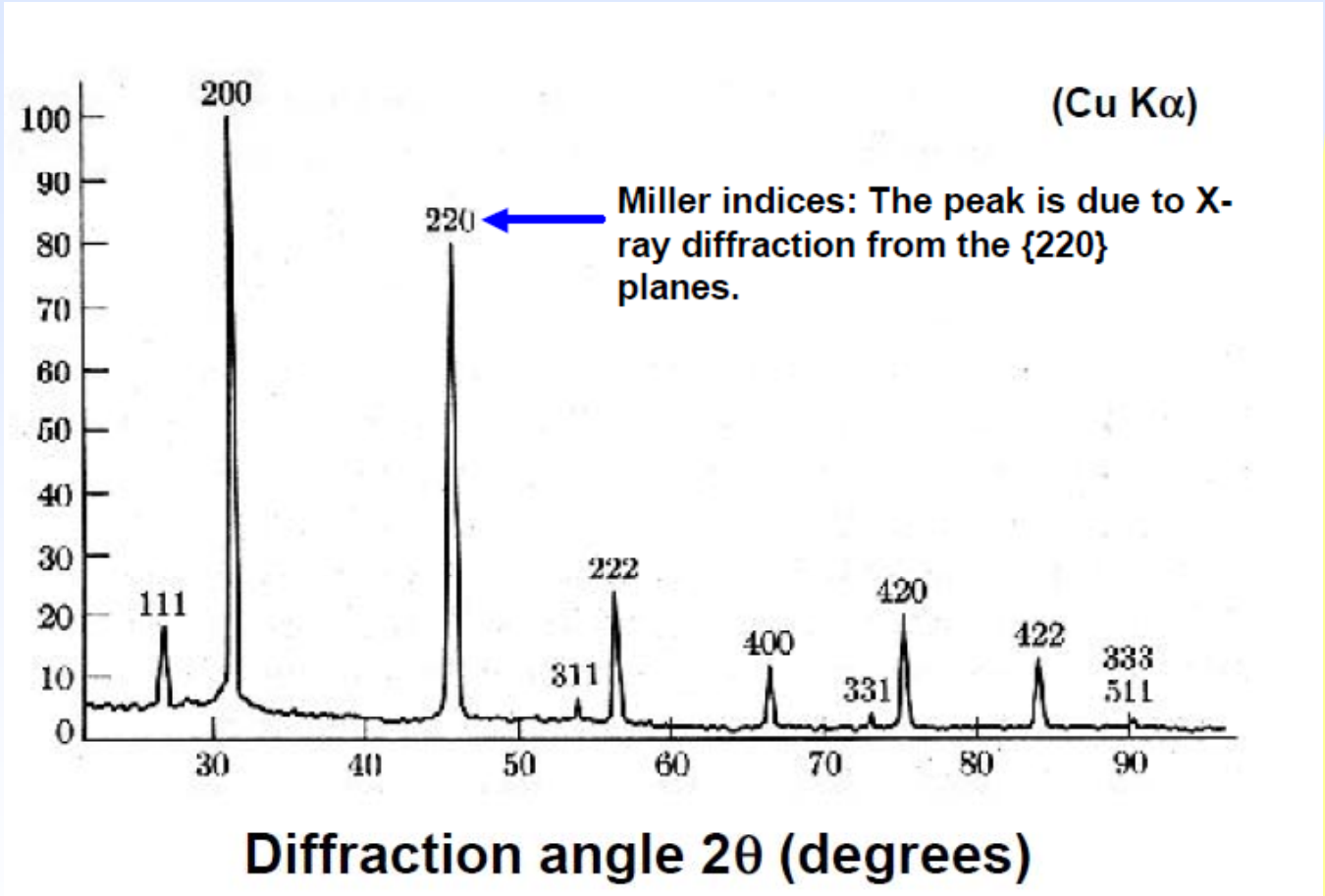

$$d_{hkl} = \frac{a_0}{\sqrt{h^2 + k^2 + l^2}}$$

LiF diffractogram (Cu K_α)

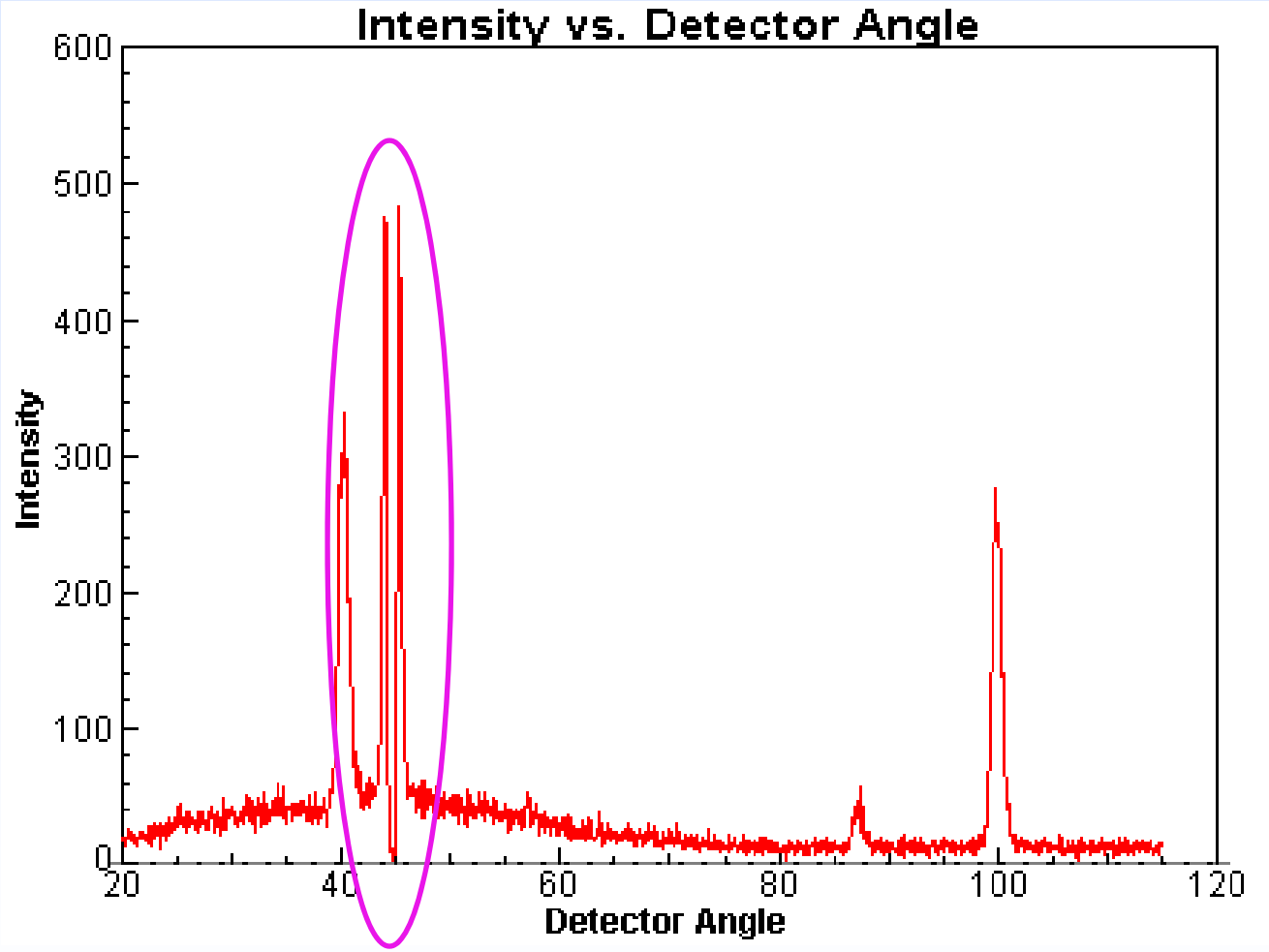

http://www.warren-wilson.edu/~physics/physics2/Formal2000/sstephens/lif.gif

Applications of XRD to NC films

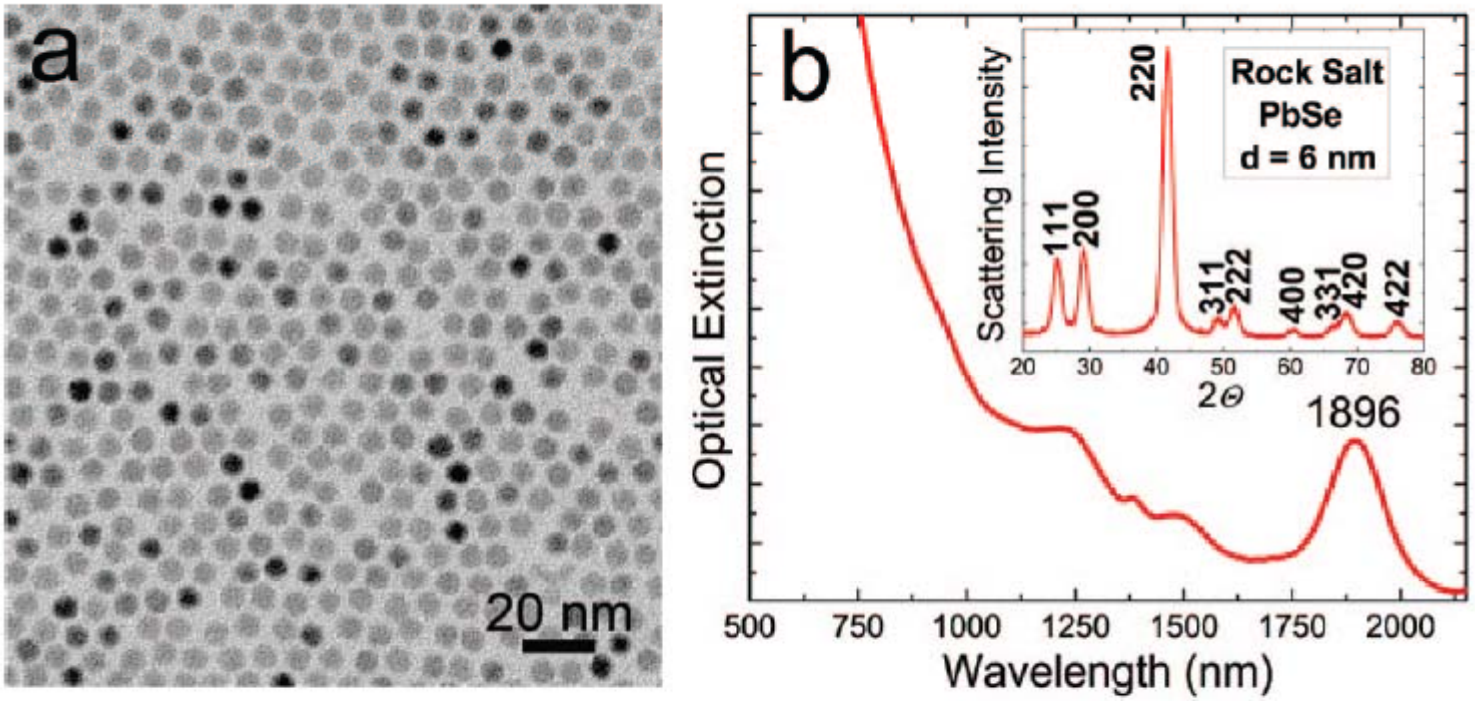

Figure 1. Basic characterization of the PbSe nanocrystals used in this study. (a) Low-resolution TEM. (b) Optical absorption spectrum of the NCs in TCE solution. The fwhm of the first exciton peak is 55 meV. Inset is the WAXS pattern of the NCs.

Law et al., J. AM. CHEM. SOC. 9 VOL. 130, NO. 18, 2008

Applications of XRD to NC films

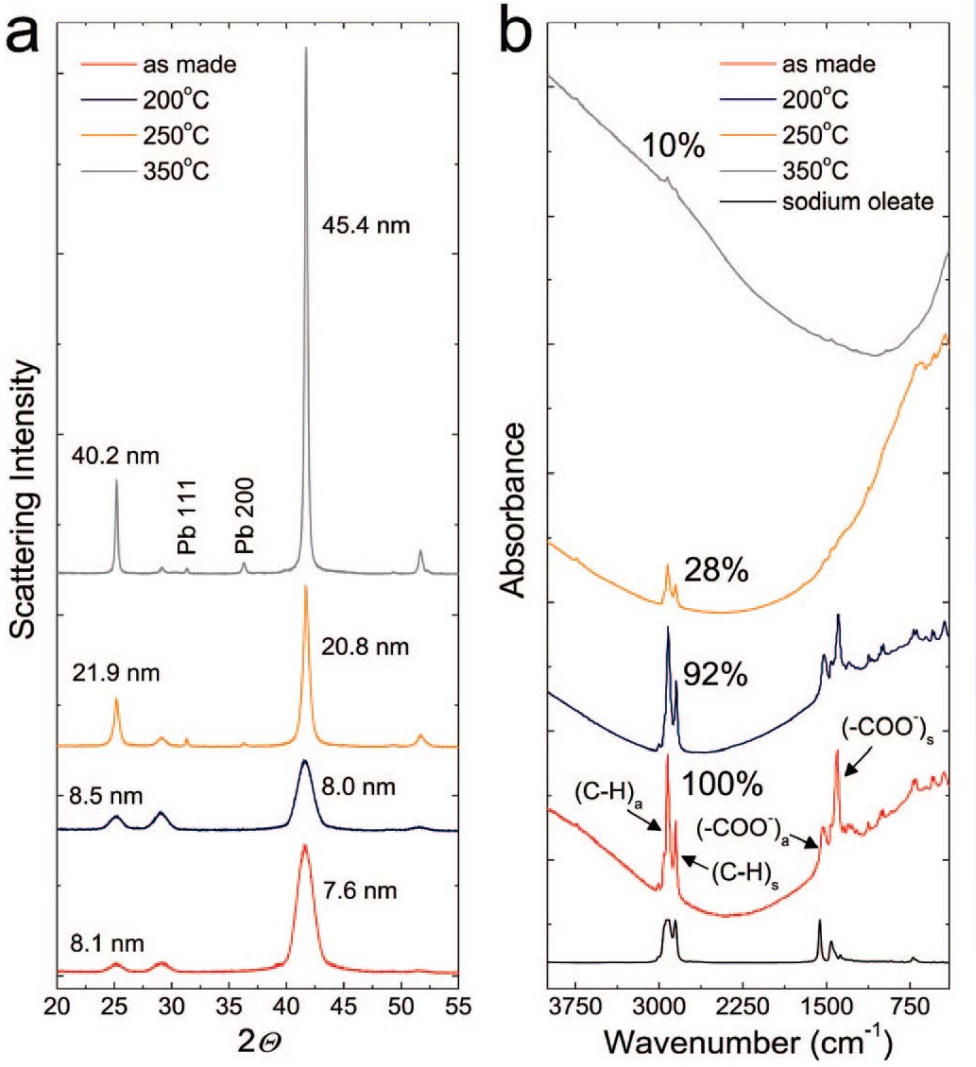

Figure 2. (a) WAXS patterns of PbSe NC films on sapphire substrates heated to 200, 250, and 350 °C. Crystalline Pb was detected with WAXS starting at 250 °C. Calculated average crystallite sizes for the 111 and 220 reflections are indicated. (b) FTIR spectra of samples on silicon substrates. A small amount of a diphenylphosphine (DPP) derivative is coadsorbed with oleate on the surface of the as-made films (out-of-plane C−H bends at 700−740 cm^{-1}, in-plane C−H bends at 990−1020 cm^{-1}). The integrated C−H stretch intensity, used to quantify the amount of oleate remaining on the films, is given as a percentage of the oleate loading of the as-made film. The sloping backgrounds are due to etaloning. A spectrum of sodium oleate is shown at the bottom for reference. These data were acquired with NCs having $\lambda_{exciton}$ = 2030 nm. The samples were exposed to air during the measurement process.

Law et al., J. AM. CHEM. SOC. 9 VOL. 130, NO. 18, 2008

Applications of XRD to NC films

Film Characterization. Transmission electron microscopy (TEM) characterization was performed on an FEI Tecnai G^2 operating at 200 keV. A JEOL JSM-7000F field emission scanning electron microscope (SEM) was used to image the films. Film thicknesses measured by SEM were corroborated with a DekTak II profilometer. Small angle and wide angle X-ray scattering measurements (SAXS and WAXS) were carried out with a Scintag X1 diffractometer (Cu Kα radiation). In WAXS, the crystallite diameter was determined from the Scherrer equation for spherical particles, $d = (K_S\lambda)/(\beta_{2\theta} \cos \theta)$ with $K_S = (4/3)(\pi/6)^{1/3}$. In situ WAXS data were acquired on a Bruker D8 Discover diffractometer utilizing a polyetheretherketone (PEEK) sample dome. Optical absorption data were acquired with a Shimadzu UV-3600 spectrophotometer equipped with an integrating sphere. Fourier transform infrared (FTIR) data were taken on a Nicolet 510 FT-IR spectrometer. X-ray photoelectron spectroscopy (XPS) was performed using a modified Physical Electronics 5600 XPS using monochromatic Al Kα radiation and a pass energy of 29 eV. The films were found

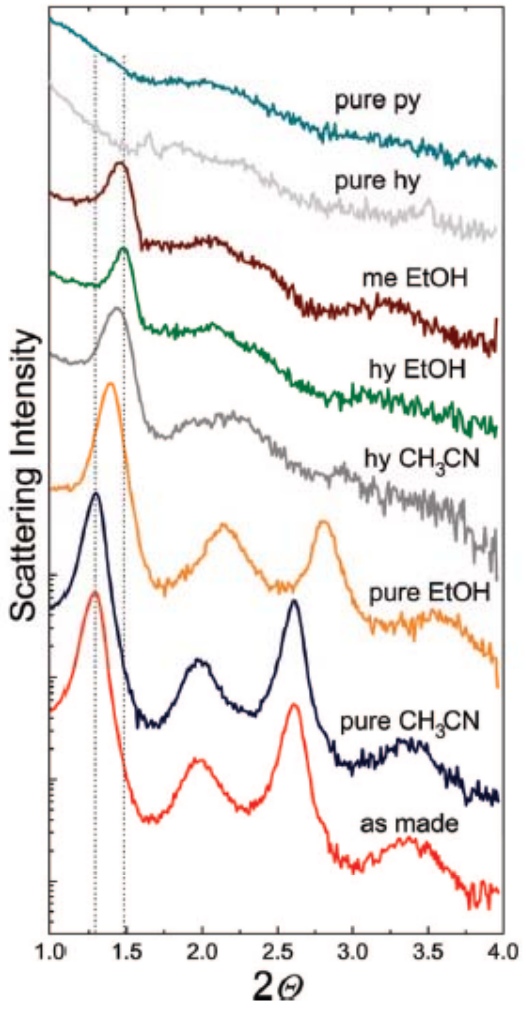

Figure 8. SAXS patterns of chemically treated films on sapphire substrates on a log-normal scale. The traces are offset for clarity. The first peak of the as-made film corresponds to first-order diffraction from close-packed layers of the nanocrystals; shifts toward higher 2Θ indicate a smaller inter-NC spacing in the packing direction along the film normal. The samples were exposed to air during the measurement process. NCs with $\lambda_{exciton}$ = 2030 nm were used in these measurements.

Law et al., J. AM. CHEM. SOC. 9 VOL. 130, NO. 18, 2008

Electro-optical characterization

ELECTRO-OPTICAL CHARACTERIZATION TECHNIQUES/CAPABILITIES

Technique/ Capability	Typical Applications	Detection Range	Temperature Range	Non-Destructive?	Image/ Mapping?
Photoluminescence spectroscopy	Determine bandgap, material quality. Identify defects	0.4–2.7 μm	4–300 K	Yes	Yes
Minority-carrier lifetime spectroscopy	Measure minority-carrier lifetime, surface recombination. Determine dominant recombination mechanism	Optical: 0.4–1.0 μm with $2x10^{-11}$ s resolution Optical: 0.4– >2.0 μm with $1x10^{-13}$ s resolution PCD: $5x10^{-9}$ s resolution	4–300 K	Yes	Yes
Fourier-transform infrared (FTIR) and Raman spectroscopy	Identify contaminants. Analyze reaction in situ. Measure impurity concentration, inhomogeneity	1.3–100 μm	8–300 K	Yes	Yes
Scanning ellipsometry	Determine film thickness, crystallinity, composition, roughness, temperature, optical and electronic properties	0.2–1.7 μm	Room temperature	Yes	Yes
Capacitance techniques	Measure carrier concentration profiles, interface state density, deep-level properties	Quasistatic to 100 MHz frequencies	77–360 K	Yes	Yes
Scanning defect mapping	Map dislocation and grain-boundary distributions in silicon wafers	10^3 to 10^8 defects/cm^2	Room temperature	No	Yes
Reflectance spectroscopy	Determine numerous solar cell physical parameters, including surface roughness, film thickness, metallization properties	Reflectance to 1% accuracy from 0.4–1.1 μm	Room temperature	Yes	Yes

http://www.nrel.gov/pv/measurements/pdfs/40121.pdf

Minority carrier lifetime measurement

High defect density decreases photogenerated (minority) carrier lifetime. Measurement of the minority carrier lifetime provides information on the material quality.

Solar Energy Materials & Solar Cells 94 (2010) 2197–2204

Contents lists available at ScienceDirect

Solar Energy Materials & Solar Cells

journal homepage: www.elsevier.com/locate/solmat

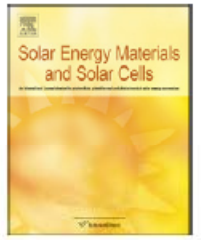

Comparison of techniques for measuring carrier lifetime in thin-film and multicrystalline photovoltaic materials

R.K. Ahrenkiel [a,b,*], N. Call [a,b], S.W. Johnston [b], W.K. Metzger [b]

[a] Department of Metallurgical and Materials Engineering, Colorado School of Mines, Golden, CO 80401, USA
[b] National Renewable Energy Laboratory, Golden, CO 80401, USA

Resonant-coupled photoconductive decay (RCPCD)

How does RCPCD work?

- Excess carriers are created by light pulses and increase the conductivity of the sample.
- Small antenna or open-ended waveguide senses changing photoconductivity in the sample.
- Electronic circuitry measures the decay of photoconductivity as carriers in the sample recombine to equilibrium concentration.

From http://www.nrel.gov/docs/fy08osti/43308.pdf

Resonant-coupled photoconductive decay (RCPCD)

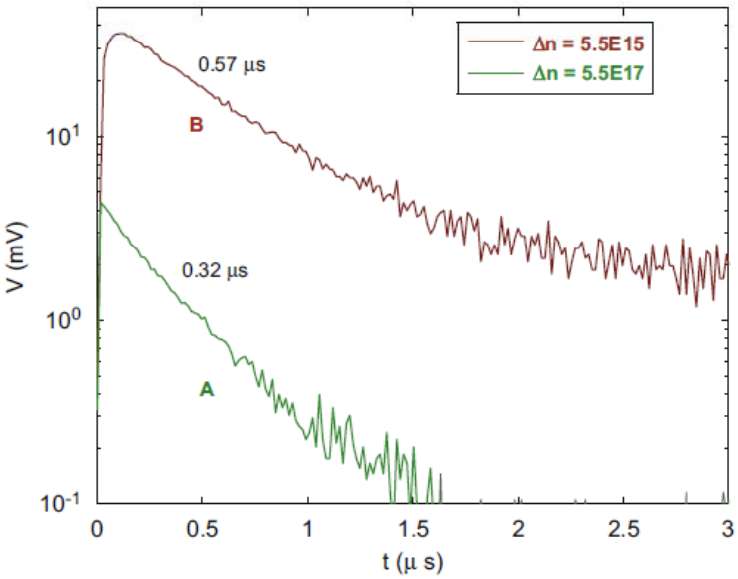

Fig. 2. RCPCD data for the sample of Fig. 1. The injection level is increased in curves A and B from 5.5×10^{15} to 5.5×10^{17} cm^{-3}. The injection level of curve B is about twice the background doping level. The space-charge reduction in the initial mobility is obvious in these data.

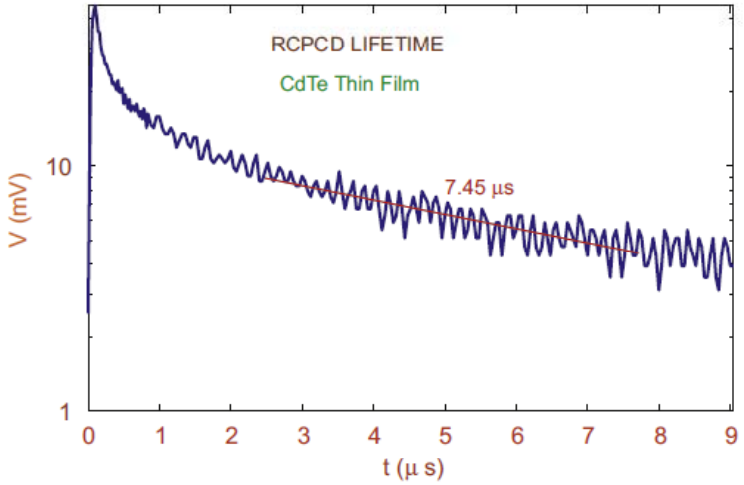

Fig. 3. RCPCD data for a high-quality, thin-film, NREL CdTe polycrystalline device grown on a glass substrate. The photoconductive decay is dominated by grain-boundary traps, whereas the recombination lifetime is about 2 ns.

3.2. *Photoconductive lifetime studies of polycrystalline thin films: CdTe*

R.K. Ahrenkiel et al. / Solar Energy Materials & Solar Cells 94 (2010) 2197–2204

Time-correlated single photon counting

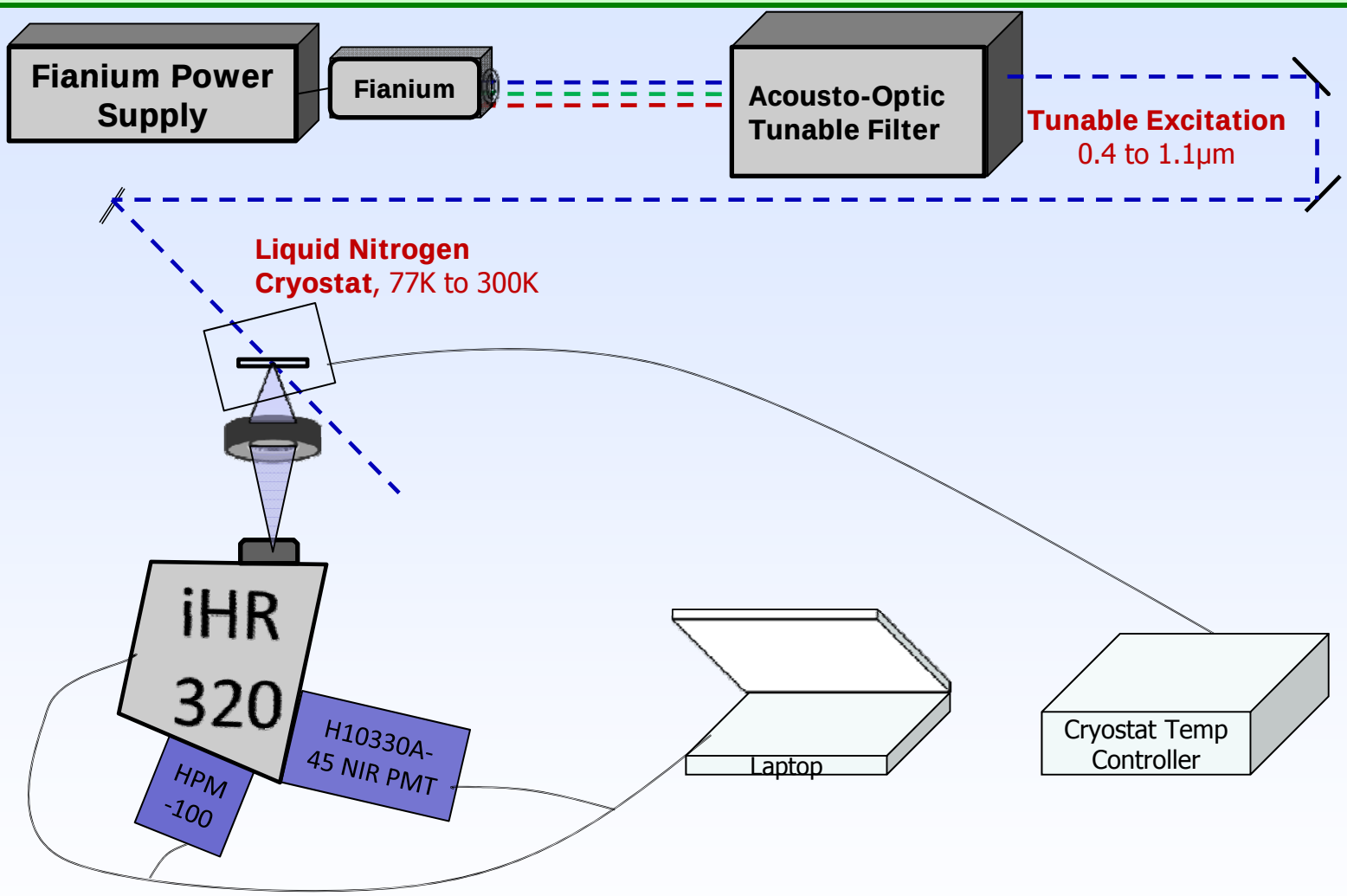

Beam Height of the iHR320 is 98mm the height of the AOTF is 26mm.

Slide prepared by N. Haugen.

TRPL Specifications

Free Space Beam Height:
AOTF: 26mm (may need a periscope)
iHR320: 98mm (from bottom of instrument?)

Temporal Pulse Width of the Fianium: ~5ps

Excitation Wavelength Range:
<420nm to >2µm from the light source, and 400nm-1100nm from the Frequency Tuner.

Detection Wavelength Range:
H10330A-45 NIR PMT: 950-1400nm
R10467U-50 Hybrid PD: 300-720nm

Transit Time Spread:
H10330A-45 NIR PMT: 400ps, Rise/Fall: 900ps/1.7ns,
R10467U-50 Hybrid PD: 90ps, Rise/Fall: 400/400ps, Width: 600ps

Pulse Rep Rate: 20MHz, 10MHz, 5MHz, 2MHz, and 1MHz

Pulse Energy: ~0.25nJ/(5nm Channel) @ 20MHz, or 2nJ with all 8 channels.

Time-resolved Photoluminescence by TCSPC

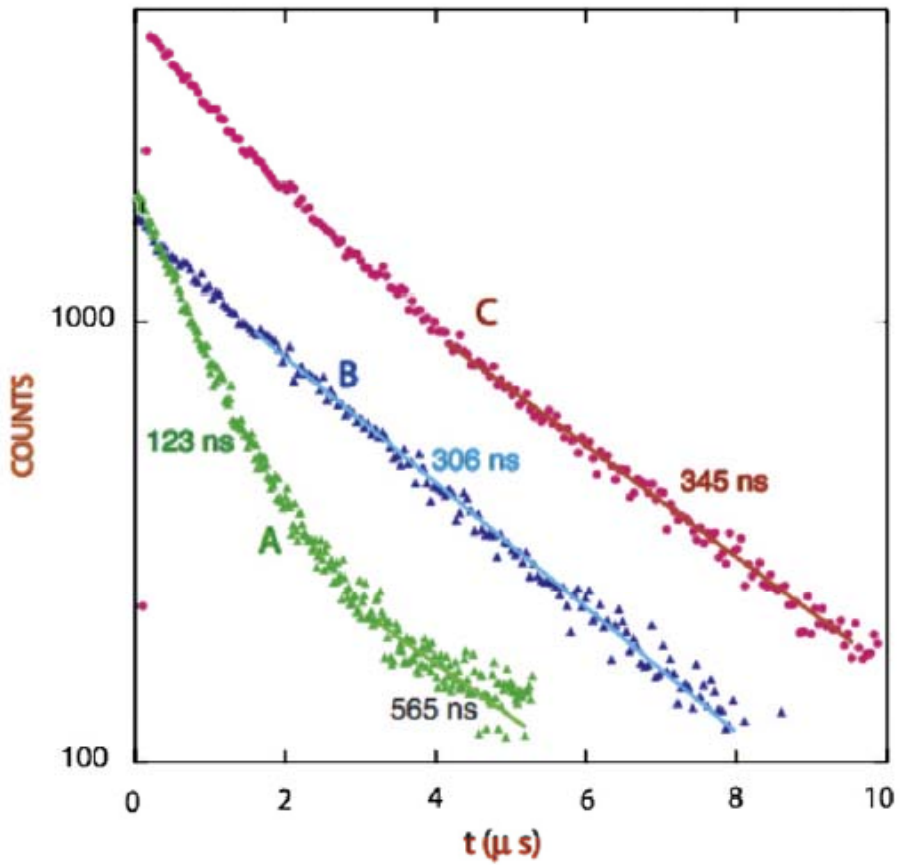

Fig. 1. TRPL data for a GaAs double-heterostructure doped p-type to about 2.4×10^{17} cm^{-3}. The injection levels in curves A, B, and C are 2.7×10^{10}, 2.7×10^{15}, and 1.6×10^{16} electrons/cm^{-3}, respectively.

R.K. Ahrenkiel et al. / Solar Energy Materials & Solar Cells 94 (2010) 2197–2204

PCD lifetime data

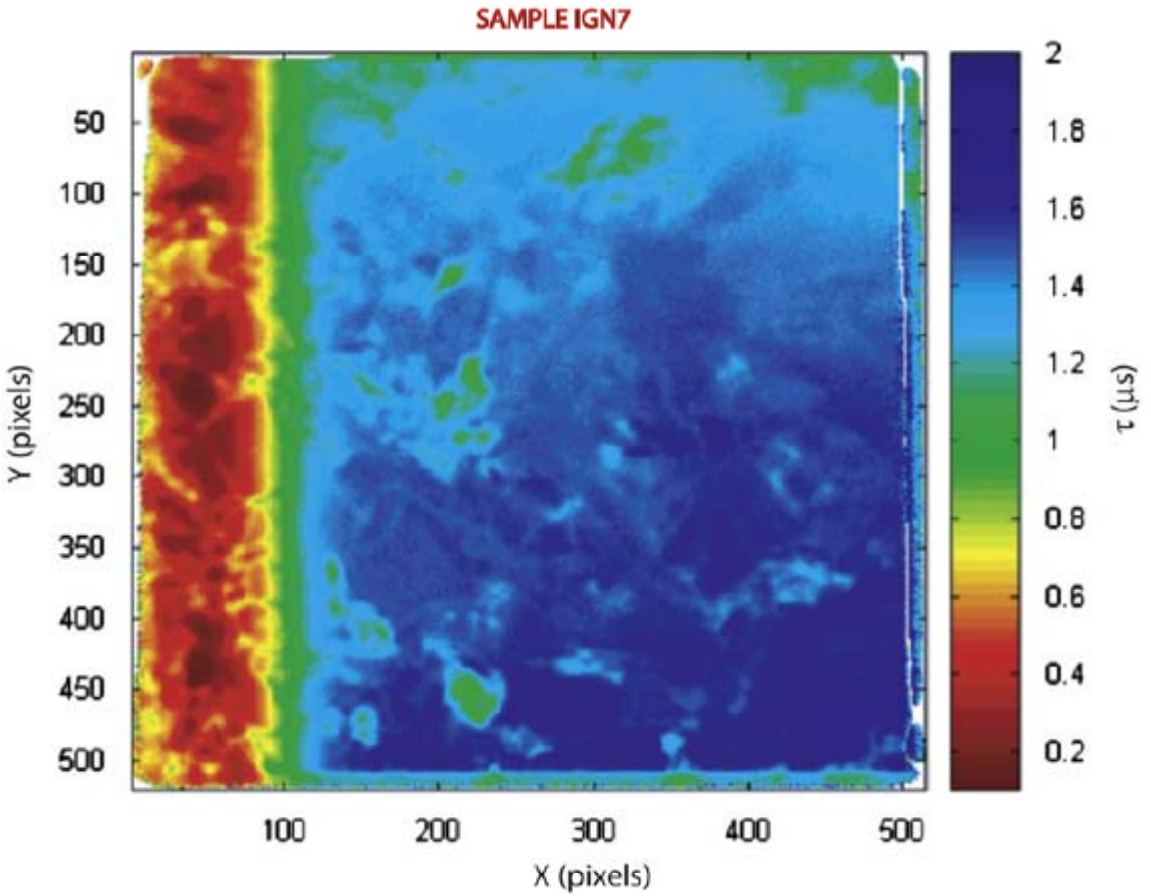

Fig. 4. The lifetime map of a 5 in. × 5 in. ingot-grown silicon wafer. The color/lifetime key in shown in the bar graph at the right of the figure. The *x* and *y* coordinates are the pixel counts in the *x* and *y* directions. Each pixel is a square of dimensions 0.25 mm × 0.25 mm. The low-lifetime region on one side is caused by contamination that occurred during the growth process.

R.K. Ahrenkiel et al. / Solar Energy Materials & Solar Cells 94 (2010) 2197–2204